**Poster2-69**

# ENERGETICS AND ROTATIONAL DYNAMICS OF HURRICANE CLUSTERS

Bryan Kerman

## SUMMARY[1]

A sequence of new results, some theoretical, others analytical, of the energetics and dynamics of cloud clusters within a hurricane, imaged by a ground-based radar, are presented.

A similarity structure for the energetics for a hurricane is first postulated, based on a theoretical analysis of the relative role of latent heating, $\dot{L}$, and dissipation, $D$, within a field of moist convection, based on the results of Pauluis and Held (2002), considered in terms of the observed probability density function (pdf) of reflectivity, $R$, for a single image of Hurricane Irma. Their ratio, $\mu = \dot{L}/D$, which is termed the convective intensity, is key to distinguishing categories, evidenced in the pdf, of the strength of convection - ranging from mixed sensible and latent heating to ultimate full latent heating.

Considerable radar meteorology research has established well-known empirical relationships between reflectivity and the (beam averaged) terminal velocity, $v_T$, droplet size, $d$, and rain rate, $RR$, which allows for estimates of dissipation, $D = g v_T$; for energy, $E = v_T^2$; and for entropy, $S = g v_t^3/\dot{L} = \mu^{-1} E$. In this description of the hurricane's energetics at pixel scale, the convective intensity, $\mu$, is synonymous with the 'temperature' of what amounts to a statistical dynamics model of the rain field.

Two methods are offered to estimate $\mu$ from the imagery. The first is through the creation of a simple physical model for the rain rate which, when compared to its estimates from its radar imagery estimate, isolates $\dot{L}$. The second is the computation of $\mu$ from the Gibbs distribution (e.g. Kerman, 1998) of the pixel-to-pixel differences in energy, with the additional assumption that the informational entropy involved is proportional to the model's entropy. Both estimates agree well over the convective range of reflectivity where the latent heating exceeds sensible heating. From this comparison, an empirical relationship is derived which allows for an explicit estimate of the convective intensity of a pixel directly from the reflectivity field.

The synonymous relationship between $\mu$ and 'temperature' allows for a computational annealing (Press et al., 1989) of the image into 'clusters'. This process mirrors the 'cooling schedule' used in the metallurgical annealing procedure in which locations of lower temperature, not hitherto attached, are attached to a warmer one, from the warmest to the coolest. The result is about 12k clusters in an image of some 140k precipitating pixels, of which 3-5k clusters are large enough to provide reliable estimates of their statistical structure. For example, the negative exponential pdf of their sizes agrees with other studies (e.g. Simpson, 1972) of (visible, distinct) cumulus cloud sizes. Further analysis is provided by the summed energetics of these clusters which shows how the various energetics and the convective intensity are distributed over the entire imaged field.

A very useful concept, entropic forces, is next borrowed from other physical processes (e.g. description of a heterogeneous field of colloids). That formulation is shown to further decompose into the two basic classes of forces in meteorological dynamics – irrotational (divergent/ convergent) and rotational (spin). Statistically the force fields over a pixel are shown to be gamma distributed and functions of $\mu$.

The two new techniques, annealing and entropic forces, are combined by summing over a cluster the implied shear stress around, and convergence into, individual pixels. The observed simultaneous existence within a cluster of counter-rotating sub-clusters suggests that there exists some self-similar process, ultimately related to the spatial distribution of local latent heating and dissipation.

A basic relationship between energy generation by $\dot{L}$ and cluster rotation is suggested from dimensional analysis, i.e. $[\dot{L}] \rightarrow v^2/t \rightarrow l^2/t^3 \rightarrow [A\,\omega^3]$ where A is the area of a cluster (or sub-cluster) and $\omega$ is its angular rotation rate. By extension one expects that the removal of energy by dissipation rate, $D$, also controls the removal of angular momentum. The ratio of positive rotational momentum, $\omega_p r_p$, in all such sub-clusters to the sum of all rotation momentum in all sub-clusters, $\omega_p r_p - \omega_n r_n$ is shown empirically to be proportional to the ratio of angular momentum generated by latent heating and that removed by dissipation, i.e.

$$\frac{\omega_p r_p}{\omega_p r_p - \omega_n r_n} \sim \frac{(\dot{L}_p r_p + \dot{L}_n r_p)^{1/3}}{(D_p r_n + D_n r_n)^{1/3}} \sim \left(\frac{r_p}{r_n}\right)^{1/3} \left(\frac{\dot{L}}{D}\right)^{1/3} \sim \left(\frac{r_p}{r_n}\right)^{1/3} \mu^{1/3}$$

The similarity constant between the ratio of positive and total angular momentum and ratio of the size compensated energy generation and dissipation is 0.66 +/- 0.026 (based on a constrained sample of 14 clusters with sizes greater than 25 pixels in order to retain sufficient numerical accuracy).

Combined with conservation of momentum, $\omega_p r_p + \omega_n r_n = \omega_{cl} r_{cl}$ and 2 other simple empirical

1 *Corresponding author address*: Bryan Kerman, 48 Albion St., Brantford, Ontario, Canada N3T 3M3, bkerman@lara.on.ca

relationships (not given here) for $r_n/r_p$ and $\omega_{cl}/\omega_p$ in terms of $\mu$ , it is possible to extract the angular rotation rates for the sub-clusters and combined cluster, and size of the sub-clusters, given $\mu, \omega_{cl}$ and $r_{cl}$ .

It is found that the vertical structure between 2 and 5km, in terms of the number of convective pixels, the number of clusters, the maximum reflectivity and the average size of clusters, is identical. This layer also demonstrates constant latent heating, dissipation as well as vertical velocity within, and peripheral stress around clusters. The average latent heating, dissipation and convectivity increase with cluster size because the latent heating increases more than the dissipation with cluster size.

In the future, it is planned to follow the time evolution and vertical structure of individual clusters. A multivariate probit method of cluster identification in subsequent, or adjacent height, images has been tested and will be applied to invariant/similar properties of individual annealed clusters.

It is remarked for interest, based on an analysis of the fractal dimension of categorized reflectivity, that a Richardson (1926) dispersion process is possibly present for the pixelated image, and has a characteristic exponent of 4/3 for weak convection and 5/3 for large convective intensity locations. A tentative model involving evolution and rotation associated with $\dot{L}$ suggests that there may exist an angular momentum exchange in a stochastic field of rotating clusters.

## 1. Introduction

The awesome beauty of radar imagery of a hurricane provides a major challenge: to understand its organized chaos, both in terms of its individual cloud structure and of the collective cloud dynamics. Basic to new understanding is having a data set which provides estimates of physical properties such as energy, entropy, force etc by which to test a model of the energetics and dynamics of a hurricane field. This paper lays out the availability of such properties from ground based radar using a similarity property controlled by a parameter which estimates the convective intensity. The concept is first developed on the hurricane's scale, then examined on the smallest available pixel scale, and ultimately applied on a cloud/cluster scale.

A new analysis technique, computational annealing, is introduced to compute a unique field of clusters The annealing process is key to being able to isolate and evaluate the energetics and dynamics at essentially the cloud level. However another new concept, entropic forces, borrowed from studies of heterogeneous materials, is first required. The combination allows for both the evaluation of the key energetics associated with latent heating and dissipation, and cluster rotation, and their interplay.

Sophisticated variables, e, g. energy, entropy etc and eventually forces, are not thought to be available on the scale of a hurricane. However, it is shown that commonly available variables provided by a radar can be combined to estimate them. The most important variables in this regard, supplied from radar reflectivity, are the estimates of rain rate, a characteristic rain drop size and a representative terminal velocity for the characteristic rain drop. From cloud physics research, it has long been established (e.g. Battan, 1973; Mali et al., 2003) that the rain rate, $\dot{R}$ , (in units of mm/h) is related empirically to the radar reflectivity, reported in units of dBz (where 0 dBz refers to the threshold of rain detection) by the equation

$$\dot{R} = \left(\frac{10^{dBz/10}}{200}\right)^{5/8} \tag{1.1}$$

and that the characteristic diameter of rain drops in the radar beam causing the reflectivity are related to the reflectivity by the relationship (e.g., Mali, 2003)

$$d = e^{0.077\, dBz - 4.04} \tag{1.2}$$

and that the terminal velocity of the droplets in the cloud mass is given by the well-known empirical equation (Rogers, 1979)

$$v_T = 6.41\, d^{0.6} \tag{1.3}$$

### 1.1 Data and Overall Procedure

Our first computational goal in Sect. 3, after examining the nature of similar hurricane energetics in Sect. 2., is to establish a relationship between these measurables, associated with the image's reflectivity, and the energetics of the clouds. In this way many aspects of the energetics can be written in these basic radar measurables and hence ultimately in terms of the reflectivity. For example, consider the following logic explored in Sect.2 that the dissipation rate is directly proportional to the heating rate associated with the condensation which is itself associated with mass (drop) production rate which is a measurable, in a form such as

$$D \Leftrightarrow \dot{L} \Leftrightarrow \dot{R} \tag{1.4}$$

Accordingly a measurement of reflectivity leads to an estimate of both the rate of dissipation and latent heating, locally, averaged over an area (pixel, cluster, hurricane).

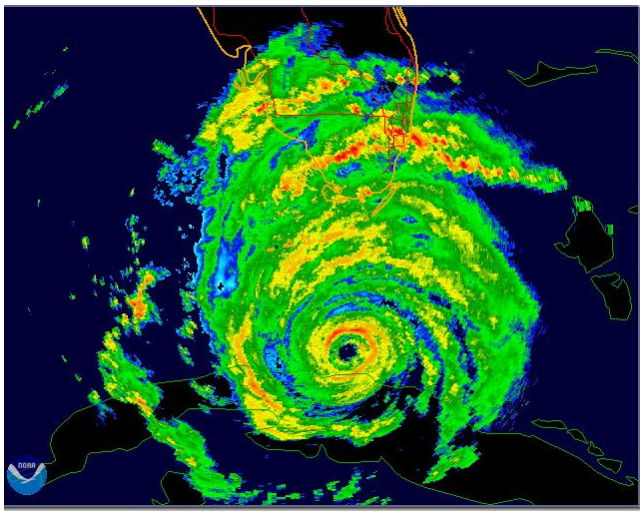

***FFigure 1a: Surface Radar Image of Hurricane Irma at 00 UDT 09/10/2017***

Consider a typical example of radar image of a hurricane (Irma) as a map of where rain-rate related dissipation is occurring within the structure. Fig 1a is an image at a height of 3000m within the core of Irma, taken by the Key West

NOAA radar. (Fig 1b is a contemporaneous satellite image.) At the time of the image, Irma was centered on the north

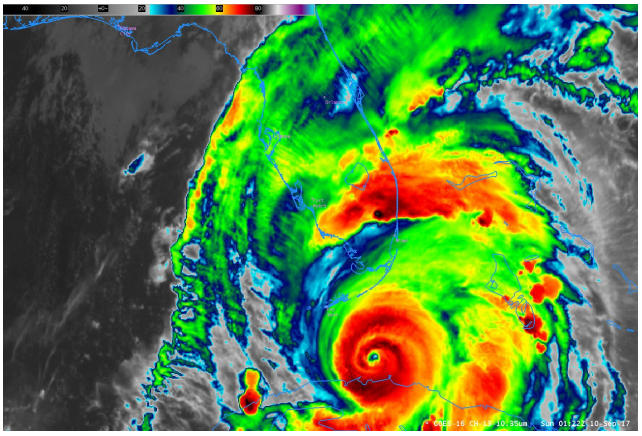

*iFigure 1b: Satellite (Goes 16) image 00 UDT 09/10/2017*

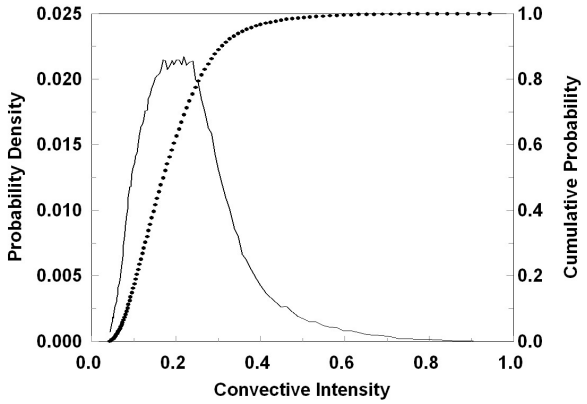


***iFigure 2: Probability density (pdf) and cumulative probability functions of radar reflectivity in Fig. 1***

coast of Cuba, just before it would soon move north-west over Key West, then up the west coast of Florida, to suddenly turn inland south of Naples, then turn north again, and begin to dissipate over land as it moved up the peninsula. There was no particular reason for this image's selection compared to an other from a time window of hours.

The image (Fig. 1a) displays an organized spatial structure, being constrained to a few sub-ranges associated with blue, green, and yellow-red coloration. Note that the three bands are embedded within each other and have a structure which occurs in concert with the other neighbouring bands. Within each band, there are chaotic structures, orientated with the band as a whole. From the dynamical point of view, discussed below, the embedding implies that there is an evolutionary path from the weak to the medium to the high convective/dissipation areas. Another feature of the image is its extended connectivity, in sinuous, elongated structures of a like colour (convective state), distinguished by subtle reflectivity differences within the band as a whole. Also, from the time animation of such hurricane imagery by NOAA, there is a dominate rotation of the hurricane as a whole, and particularly of the bands as major elements within that imagery. In summary a subjective analysis of the image indicates distinct states of convective activity, embedded in each other, with smaller scale structure itself embedded in a convectively weaker state, with a superimposed overall rotation for the entire hurricane.

The basic nature of the overall convective field is usefully analyzed in terms of a histogram of the reflectivity. The normalized histogram, or probability density function, hereafter pdf, of the image is shown in Fig. 2. It is immediately apparent that the three major colour states correspond to three distinct regions of reflectivity/convective activity, often referred to, variously, as weak/shallow, moderate/congestus and strong/deep convection.

The immediate challenge is to provide an explanation for this probabilistic structure of the imagery in terms of the energetics of the whole cloud field of the hurricane that will eventually allow both identification of individual convective structures, and the mesoscale field they are embedded in, both kinematically and dynamically.

However before proceeding, a definition of 'state', as used below, is required that is compatible with the processes at the large, hurricane scale and at the much smaller cloud level. Accordingly, a state is defined as those locations (pixels, clusters) within given limits $(\mu_{low}, \mu_{high})$ of the convective intensity (defined below). The state need not be a contiguous area but the imagery suggests that there are major areas of identical state properties. A mean state variable within a state, with a given convective intensity, i.e. within a range $(\mu_{low} < \mu < \mu_{high})$, for example the state latent heating rate, $\dot{L}_s(\mu)$, is then understood to be that of all pixels (later clusters) in that state i.e.,

$$\dot{L}_s(\mu) = \dot{L}(\mu) \qquad (1.5)$$

Further, and as discussed in more detail below, it is also assumed in the overall development that there is a similarity (i.e. proportionality) correspondence between all variables, such as mass, energy, dissipation rate and entropy, both on an individual pixel basis and collectively, under the (convective intensity) parameter. Accordingly these similarity functions provide insight into how the convective field evolved from one state to another with increasing convective intensity, and the local differences implied at a point or area in the imagery.

## 2. Similarity Model of Hurricane Scale Energetics

Consider a model of the balance of energy creation and removal by various contributing processes on the ensemble of pixels in a hurricane at a given height. The formulation and major balances of both energy and entropy in a moist atmosphere, follow from discussions by Pauluis and Held (2002), (hereafter PH), as well as Craig (1996), Bister and Emanuel (1998), and Kleidon (2010) as well as scaling discussions by Emanuel and Bister (1996), and equilibrium discussions by Tao et al. (1999). A major outcome, based on order of magnitude considerations by PH and others is that the dissipation associated with jostling rain drops is significantly larger than the dissipation associated with dry air, kinetic energy (Kolmogorov) turbulence. Here energetics considerations in this work differ from these previous analyses in that the are examined on the evidence for 3 distinct states. The development considers the dissipation rate as the independent variable, when in fact it is a

dependent variable in that other factors determine the dissipation, not the opposite.

Consider now two major relationships developed by PH for energy and entropy change within a moist, convective atmosphere, which a hurricane certainly is. For energy, $E$, there is a balance, exclusive of large scale interactions, such as radiative effects, given by

$$\frac{dE}{dt} = \dot{E} + W_{sen} + W_{vap} - (D_p - D_t) \tag{2.1}$$

where $(W_{sen}, W_{vap})$ are the work done by the volumetric expansions due to the addition of thermal (sensible) and evaporative (water vapour) heat originating from the surface; and $(D_p, D_t)$ are the dissipation rates due to rain and Kolmogorov turbulence. At cloud height $W_{vap}$ is the work done by the water vapour pressure in the vicinity of the cloud. Note that the energy budget does not include the latent heating explicitly in Eq. 2.1.

The entropy, S, balance, again exclusive of external effects, is given by

$$\frac{dS}{dt} \equiv \dot{S} = \dot{L} + W_{sen} + W_{vap} + (D_p + D_t) \tag{2.2}$$

where $\dot{L}$ is the latent heating within the clouds. For a constant energy process the relationship for entropy change is reduced to

$$\dot{S} = \dot{L} + 2(D_p + D_t) \tag{2.3}$$

Of the numerous length scales associated with the convective process, consider two which describe the energetics of a rain drop at its terminal velocity and during the evolution of a cloud itself. The first is the distance a characteristic droplet will fall before it stops accelerating, given by $\lambda_{dr} = v_T / g$. The other length, $\lambda_{cl} = v_T^3 / \dot{L}$ ,describes the characteristic size of the cloud's mixing zone, driven by the latent heating. The ratio of these length scales,

$$\mu = \frac{\lambda_{dr}}{\lambda_{cl}} = \frac{\dot{L}}{g v_T} \tag{2.4}$$

is a measure of the relative strength of latent heating and dissipation, and is defined as convective intensity. The value of $\mu$ ranges from essentially 0 in the lower limit of weak (shallow) convection to 1 in the upper limit of strong (deep) convection, as shown below (Eq. 2.17).

It is argued that the cloud mass is in a steady, or nearly steady, (equilibrium) energy state at any $\mu$ which in Eq. 2.3 is expressed as a balance between work associated with sensible heating and another associated with the delivery of water vapour, and dissipation contributions associated with each process, given by

$$W_{sen} + W_{vap} = D_p + D_t \tag{2.5}$$

(Note that in the above, by convention, a dissipation rate is treated as positive whereas physically it is negative.)

Aside from the entropy decrease associated with radiation from clouds (not discussed here), the entropy associated with cloud generation, rain production, and dissipation increases, i.e.

$$\dot{S} > 0 \tag{2.6}$$

for $\Delta t > 0$ which is equivalent to $\Delta \mu > 0$ . As shown below, the monotonically increasing entropy is intertwined with an increase in convective intensity so that a discussion of increasing convective intensity implies increasing disorder, in the sense of the observation of rare events such as localized, very energetic structures.

We now consider the energetics of each of the three states in more detail. To emphasize which state is being described, a leading subscript with the state number is used.

## 2.1 State 1: Weak (Shallow) Convection

Order of magnitude calculations indicate that ${}_1W_{sen} \ll {}_1W_{vap}$ over most of the weak convective process, with one important caveat. In the case of very weak convection, when the rain rate and its associated dissipation rate are also very small, there is vanishingly small work done by the vapour flux, i.e., ${}_1W_{vap} \to 0$ . In this narrow range of convective intensity, the sensible heating, i.e. ${}_1W_{sen}$ , dominates. Conversely in the weak convection state for larger dissipation rates, ${}_1W_{vap} \to {}_1D_p$ and ${}_1W_{sen} \to 0$ .

However that argument is flawed as it does not account explicitly for the effect of latent heating as a (weak but increasingly important) source of energy. Accordingly two parallel processes are delineated in State 1 whose net effect maintains the boundary conditions. The first partition represents the sub-process not affected by latent heating, written as

$${}_1W_{sen} + {}_1\hat{W}_{vap} = {}_1\hat{D}_p + D_p \tag{2.7}$$

where $({}_1\hat{W}_{vap}, {}_1\hat{D}_p)$ are the sub-process work and dissipation rate. It is assumed that this process of decreasing sensible and increasing vapour heating is almost in balance, so that a sum of combined sensible and vapour work is almost constant at the sensible work at cloud initiation.

The other sub-process represents the very small affect of latent heat in this sensible heat dominated state. Although small, the latent heating will require an additional supply of vapour, expressed as

$${}_1\widetilde{W}_{vap} = {}_1\dot{L} \tag{2.8}$$

The combined result for the work associated with water vapour in the two sub-processes, which must equal the original water vapour work, if a steady state is to be maintained, is given by

$${}_1W_{vap} = {}_1\hat{W}_{vap} + {}_1\widetilde{W}_{vap} \tag{2.9}$$

It follows from the combined dissipation rates that

$${}_1D_p + {}_1\dot{L} = {}_{1,2}D_p \tag{2.10}$$

where ${}_{1,2}D_p$ is the (total) dissipation rate at the critical convective intensity, occurring at the juncture of states 1 and 2. The combined balance to satisfy energy conservation becomes

$$D_1(\mu = 0) = {}_1W_{sen}(\mu = 0) = {}_1\hat{W}_{vap}(\mu_{1,2}) + {}_1\widetilde{W}_{vap}(\mu_{1,2}) = D_p(\mu_{1,2}) \tag{2.11}$$

Eq. 2.11 also provides estimates for $(D_t, {}_1W_{sen})$ at $\mu = 0$ . From Fig. 2, empirically $\mu_{1,2} = 0.17$ , and the associated (calculated) dissipation rate is 16.3 W/kg at 24 dBz. Also, from the cumulative probability function (cpf) plot in Fig. 2, weak convection occupies in about 50% of the image.

Originally $\mu_{1,2}$ was identified on the basis of a distinct change in the number of pixels with increasing convective intensity. The assumptions and arguments imbued in the model collectively describe the energetics of the two constrained sub-states within State 1 combined in such a way as to maintain a steady state. For convective intensities in State 2, the number of pixels remains relatively constant. Apparently the achievement of what amounts to a minuscule latent heating in State 1 controls the number of pixels exiting State 1 and entering State 2.

### 2.2 State 2: Moderate (Congestus) Convection

The most significant characteristic of this state is that the number of pixels at any convective intensity do not increase or decrease significantly and the number of pixels established in State 1 is roughly maintained. This unexpected result requires an explanation. It is argued that those pixels emanating from State 1 are replaced by pixels of higher convective intensity associated with State 2, not necessarily in a migration across State 2, but within the state as a whole. Such a procedure requires an organized replacement process such that pixels incubated in State 1, are intensified, perhaps to varying degrees, but such that the replacement continues to lie within State 2.

Consider the deduced energetics of State 2 which from Fig. 2 occupies about 25% of the hurricane's area. The critical convective intensities are estimated to be $\mu_{1,2} = 0.17$, as mentioned above, and $\mu_{2,3} = 0.24$. (The latter occurs at a reflectivity of 29.5 dBz with a deduced dissipation rate of 21.5 W/kg). As in the considerations of State 1, a steady state is assumed, which in the absence of sensible heating effects in State 2, requires

$$ {}_2W_{vap} = {}_2D_p \qquad (2.12)$$

As postulated for State 1, it is argued that two embedded sub-processes exist such that

$$ {}_2W_{vap} = {}_2\hat{W}_{vap} + {}_2\widetilde{W}_{vap} \quad \text{and} \quad {}_2D_p = {}_2\hat{D}_p + {}_2\widetilde{D}_p \qquad (2.13)$$

Further, if the latent heating is to be balanced such that

$$ {}_2\widetilde{W}_{vap} = {}_2\widetilde{D}_p = {}_2\dot{L} = \mu_{2,3} D_p(\mu_{1,2}) \qquad (2.14)$$

and that part of the water vapour work, not associated with support for the latent heating, must be a fraction, $(1-\mu_{2,3} = 0.76)$ of the dissipation rate, or about a factor of 3 compared to latent heating.

This hypothesized partition provides a reasonable (linear) approximation for the behaviour of the latent heat and work by water vapour given by

$$ {}_2W_{vap}(\mu) = {}_1W_{vap}(\mu_{1,2}) + (1-\mu_{2,3}) \frac{\mu-\mu_{1,2}}{\mu_{2,3}-\mu_{1,2}} {}_2D_p(\mu) \qquad (2.15)$$

and

$$ {}_2\dot{L}(\mu) = \dot{L}_1(\mu_{1,2}) + \mu_{2,3} \frac{\mu-\mu_{1,2}}{\mu_{2,3}-\mu_{1,2}} {}_2D_p(\mu) \qquad (2.16)$$

### 2.3 State 3: Strong (Deep) Convection

From Fig. 2, there is evidence of a fundamental change at $\mu_{2,3}$ in the number of pixels at that convective intensity. The significant decrease in the number per dBz interval suggests an altered energy balance in State 3. As in States 1 and 2, a steady state can be maintained if there is an exchange between the water vapour work and the latent heat. The reduction of pixels with increasing convective intensity suggests that above $\mu_{1,2}$ the morphology of the cloud masses changes to support the provision of more energy into more active cores.

Hitherto no reference has been made to the entrainment of convective available potential energy (CAPE) with increasing convective intensity. It is argued that increased kinetic energy for stronger updrafts is provided from the CAPE which in turn draws more water vapour from the low levels into the convective core, and increases latent heating. Eventually, at maximum convective intensity, the process is solely driven by the latent heating, originating from the CAPE, expressed in the equation chain

$$ CAPE = {}_3W_{vap} = {}_3\dot{L} = {}_3D_p(\mu_{max}) \qquad (2.17)$$

where by definition $\mu_{max} = 1$. It is further argued that, at convective intensities between $\mu_{2,3}$ and $\mu_{max}$, the CAPE accessed by the turbulent kinetic energy is just enough to induce latent heating, ${}_3\mu_3 D_p$, and water vapour work, $(1-\mu_3)_3 D_p$ to maintain in a steady state.

It is useful to summarize the increase in entropy at various critical convective intensities.

At $\mu_{max}$ $$ \dot{S}_{max} = \dot{L} + D_p = 2D_p(\mu_{max}) \qquad (2.18)$$

and at $\mu_{2,3}$ $$ \dot{S}_{2.3} = \dot{L}_{2,3} + 2D_p(\mu_{2,3}) \qquad (2.19)$$

and at $\mu_{1,2}$ $$ \dot{S}_{1,2} = \dot{L}_{1,2} + 4D_p(\mu_{1.2}) \qquad (2.20)$$

The fractional contribution of latent heating to dissipation, $\mu = \dot{L}/D_p$, to the rate of entropy increase, varies from 4 to 1. It is reasonable to expect that the proportionality of various energy changing processes on the hurricane scale are similarity functions under a similarity argument $\mu$.

## 3. Similarity Cloud Model

We now turn to evaluating hurricane energetics, ultimately using radar imagery, at the pixel scale, based on the previous hurricane scale model.

Consider initially the collective energetics of convective clouds. The process involves the removal of heat associated with the condensation around nuclei, to form seeds which in turn grow by accretion upon collisions to produce droplets some of which are heavy enough to escape the turbulent core of a cloud and fall as rain. The key variables which describe this process are the terminal velocity, $v_T$, of a characteristic drop of diameter, $d$, chaotically falling and rising thorough a turbulent field driven by gravity, $g$, and buoyant vertical updrafts induced by the latent heating, at a rate, $\dot{L}$, of the air around the condensing droplets.

These variables $(d, g, v_T, \dot{L})$ form the basis of similarity relationships for the major pixel-scale energetics. The simplest energetics variable, representable in terms of radar measurables is the dissipation rate, $D = g v_T$, so that the balance involved in driving the turbulent precipitation field, between the rate of latent heating and the dissipation, is conveyed in the convective intensity

$$ \mu = \frac{\dot{L}}{g v_T} \qquad (3.1)$$

These base variables also form two sets of characteristic time and length scales. The first set which describes the faster and smaller process associated with drop creation is given by $(\tau_{dr} \sim v_T/g, \lambda_{dr} \sim v_T^2/g)$ and the second set which describes the characteristic roll-over time and spatial extent of the cloud's turbulent core given by $(\tau_{cl} \sim v_T^2/\dot{L}, \lambda_{cl} \sim v_T^3/\dot{L})$. Another non-dimensional number, $d/\lambda_{dr}$, is a measure of the efficiency of the accretion process in the surrounding turbulent field. The internal process time constant, $\tau_{dr}$, is hypothesized to be independent of the overall local convective intensity while the turn-over process time scale is a function through the effect of $\dot{L}(\mu)$.

### 3.1 Model of Rain Rate

A similarity relationship for the rain rate, $\dot{R}$, is sought in the form, $\dot{R} = v_T \Psi_R(\mu)$ by constructing the following model and determining the functional form of $\Psi_R$. Visualize the bottom of a cloud of spatial area, $\lambda_{cl}$, with 'holes' of size, $\pi/4\, d^2$. Consider a shaft above the drop exit of length, $\lambda_{dr} \sim v_T^2/g$, which produces a droplet at a time delay, $t_{dr} \sim v_T/g$ after an initiation occurs, randomly over all the shafts, so that a droplet falls down a 'shaft' and out the bottom of the cloud. The concept is that a seed initiated at height, will grow to a droplet of size, $d$, and then exit the cloud. The random initiation occurs at a rate, $t_{cl} \sim v_T^2/\dot{L}$ associated with the turbulent field above the interfacial layer at the cloud base. The result is a shaft of length, $\lambda_{dr}$, and area $\pi d^2/4$ that is released every $\tau_{cr}$, containing a drop of volume, $\pi d^3/6$. The cloud base rain rate (per unit area) is the expulsion volume divided by the expulsion area, i.e. $2d/3$ occurring in a time interval, characteristic of the roll over of the core of the cloud. Assuming there is negligible evaporation from cloud base to the surface, so that the cloud base and surface based rain rates are identical, the result, within geometric and scaling factors, is

$$\dot{R} \sim \frac{d}{\tau_{cl}} = \gamma(\mu)\frac{gd}{v_T}\left(\frac{\dot{L}}{g v_T}\right) = \gamma(\mu)\frac{g d}{v_T}\mu = \gamma(\mu)\frac{g d}{v_T}\mu \qquad (3.2)$$

The factor $\gamma(\mu)$ represents both a geometric coefficient, 2/3, and the real dynamics associated with the mass creation process which occurs across a spectrum of drop sizes and terminal velocities and is expected to be a monotonically increasing function of μ. The simplest estimate of $\gamma$ is $\gamma \sim \alpha^{-2}\mu$ where $\alpha$ is a scaling constant. Accordingly the convective state can be derived from the rain rate

$$\mu = \alpha\left(\frac{v_T}{gd}\dot{R}\right)^{1/2} \qquad (3.3)$$

and the latent heating from the definition of $\mu$. The scaling constant, $\alpha$, calculated from $(gd/v_T\dot{R})^{1/2}$ at $\mu = \mu_{max} = 1$, i.e. at maximum reflectivity, is 7.85.

### 3.2 Temperature Analogy Model

A second method exists for an indirect determination of $\mu$ which is based on an estimate of informational entropy from the conditional probability, $p_c$, of differences of a measure of energy, $\delta e$, with nearest neighbours (e.g. Kerman, 1998). It is invariably found that the distribution of informational entropy, $-\ln(p_c)$, is a negative exponential in the form $-\ln p_c = \epsilon\,\delta e$ where $\epsilon$ links the energy to the informational entropy. Such a procedure was undertaken (Appendix A), based on the similarity solution between entropy and energy (Eq. 3.8 below) to compute $\mu$.

Based on the empirical results analyzed there, it is argued that there are reasonable grounds to assume that informational entropy is proportional to the physical entropy field, so that $\epsilon = \beta\mu$. The proportionality constant, $\beta = 14.5$, was obtained by scaling the maximum $\epsilon$ (Fig. 3) to bring the implied maximum convective intensity to 1 at maximum reflectivity.

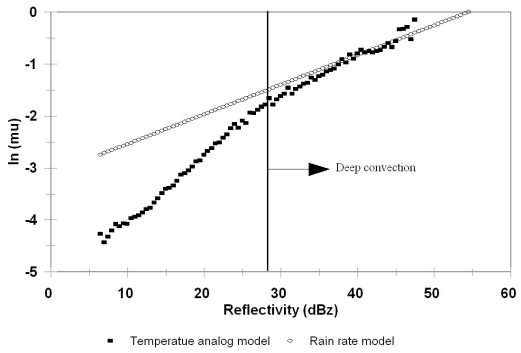


***iFigure 3: Convective intensity as a function of radar rreflectivity***

While the rain rate model (Eq. 3.3) is in agreement with temperature analogy model in the deep convection state, the two results differ in the low and medium convective intensity states. This implies that the assumption of informational and physical entropy proportionality is at least correct for the deep convection state. The divergence of the results for weaker convection is therefore due either to failure of the assumption on the form of $\gamma(\mu)$ (see Eq. 3.2) in the rain rate model or failure of the assumption of informational and physical entropy. Because there is both informational entropy change associated with cloud morphology and physical entropy change at the congestus/ deep state critical convective intensity leads to the conclusion that the temperature analogy developed in Appendix A is more realistic than rain rate model, which is limited to deep convection.

The two line segments seen in Fig. 3 can be empirically represented by

$$\mu = .0919\left(R/R_{max}\right)^{0.948} \qquad (3.4)$$

for very weak (sensible heat dominated) convection (state 1) ( $R/R_{max} \le 0.23$ ) and $\mu = \left(R/R_{max}\right)^{2.556}$ (3.5)

for the congestus and deep convection (states 2 and 3), where $R_{max}$ is the maximum reflectivity in the image.

These derivations by which to relate the convective intensity to reflectivity are very useful because they allow for the crucial estimate of $\dot{L}$ from radar measurables, which has hitherto not been possible. Also an estimate of $\mu$, allows for the derivation of two other important variables, the spatial, and ultimately temporal, distribution of mass and entropy within the imagery discussed next.

### 3.2 Similarity Structure of Cloud Energetics

To estimate force, energy, dissipation and entropy, it is useful to develop a relationship for $m$, the mass of droplets suspended in a cloud. Consider the following chain of approximations for $m$, in terms of a cloud scale roll-over, given by

$$m = \dot{m}_{dr}\,\tau_{cl} = \rho_w\left(\dot{R}\,\lambda_{dr}^2\right)\tau_{cl} \sim \rho_w \frac{v_T^4 d}{g^2}\mu \qquad (3.6)$$

Consider also the similarity relationships for other variables per unit mass

: for vertical acceleration $a = g$ (3.7)

: for energy

$$E = A\,\lambda_d = v_T^2 \qquad (3.8)$$

: for dissipation rate

$$D = \dot{E} = E\,\tau_d^{-1} = g\,v_T \qquad (3.9)$$

: for entropy

$$S = \dot{S}\,\tau_{cl} = D\,\tau_{cl} = \mu^{-1} v_T^2 = \mu^{-1} E = \frac{g\,v_T^3}{\dot{L}} \qquad (3.10)$$

It is worth noting that the various representations for acceleration, turbulent kinetic energy and dissipation rate have no explicit scaling in $\dot{L}$ or the convective intensity, $\mu$. Where the similarity scaling does explicitly include $\mu$, in the similarity relationship for entropy (Eq. 3.10), the relationship is continuous in $\mu$, but discontinuous in reflectivity as discussed above. Because any analysis will necessarily be conducted, at least initially, on the basis of the reflectivity this discontinuity is apparent in other analyses.

In summary, the model above offers a simple method, starting with basic variables sensed by a radar, $(d, v_T, \dot{R})$, by allowing for the computation of $\dot{L}$, to the provide estimates of energy, dissipation and entropy. In essence Eqs. 3.7 to 3.10 decode the reflectivity field to the energetics of a hurricane at pixel scale.

## 4. Cloud Clusters by Simulated Annealing

While a radar senses areas of precipitation, it does not inherently identify organized cloud areas. A technique which examines the logical arrangement of a reflectivity field and sorts out mutually unconnected clusters is discussed next. Simulated annealing (Press et al.,1989) computationally mimics the physical process of metallurgical annealing which cools heated metals sufficiently slowly to achieve an optimally different `temper`, or fine grain arrangement. Sometimes called computational annealing, the only `computations` are logical comparisons, ideally of `temperature` but generally, of any energetic variable related monotonically to the `temperature`. The objective is to attain an equivalent slowest cooling by attaching `warmer` locations (pixels) to a minimally cooler location.

The computation plan identifies locations by their temperature (or energy state), and places them in descending order in a `cluster map. If they are placed without a selected neighbour they become the seed for a new cluster. If the location of the selection is adjacent to an already collected pixel they are attached to that cluster thus allowing the existing island (cluster) to `grow`. Only when no unattached pixels surround a cluster does it stop growing, Restated, the annealing process draws on a sorted list/ annealing schedule and builds a locally connected sub-state by attaching neighbouring pixels at a lower `temperature`. When annealing the hurricane imagery, the convective intensity of each location forms an obvious analog of temperature to construct the annealing schedule

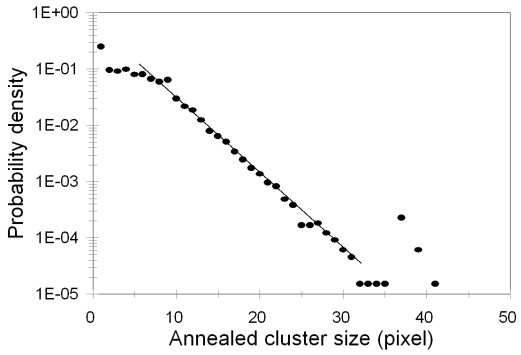


***Figure 4: Probability density function of the size of clusters formed by annealing the convective intensity, $\mu$, field.***

The image from Hurricane Irma (Fig. 1a) contains about 128k locations/pixels indicating precipitation. The annealing process results in about 12k clusters which are distributed in size as shown in Fig. 4 which indicates that many clusters are less than about 8-10 pixels in size. The outstanding question about these clusters is 'Are they real physical identities?'. The first proof that they are is the observed negative exponential form of their probability distribution for sufficiently large clusters, above 10 pixels, which is similar to observed cloud size distributions (Simpson, 1972). The second is their coherence when isolated in radar images at subsequent times and neighbouring heights. The third and most significant reason to believe they are physical structures lies in the implied rich dynamics within a cluster as discussed below.

## 5. Implied Cluster Forces

A radar hurricane image also supplies estimates of the force field around pixels, and within and around the periphery of clusters. Entropic forces are defined in terms of the gradient of entropy of a field recognizing that forces within a system will be in the direction of entropy maximization. The concept has been successfully applied in studies of the heterogeneous properties of materials, such as colloids.

The entropic (vector) force between pixels of different entropy, $S$, is defined as

$$\vec{a_H} = \mu \frac{\partial S}{\partial \vec{x}} = \frac{\partial E}{\partial \vec{x}} - S\frac{\partial \mu}{\partial \vec{x}} \quad (5.1)$$

which expands to

$$\vec{a_H} = \frac{\partial v_T^2}{\partial \vec{x}} + v_T^2 \frac{\partial \ln \mu}{\partial \vec{x}} \quad (5.2)$$

The first term is conservative in that it will integrate to 0 around any closed path (such as the edge of a pixel) no matter the details of the path, and is irrotational. The second term is rotational as its integral is non-zero if $v_T^2 > 0$ (which is guaranteed) and uncorrelated with $\ln \mu$ along the integrals path. As will be seen below, the irrotational acceleration is associated with a self-organized process driven by radial (convergent/divergent) forces and the rotational acceleration with a cluster rotation. In both cases the direction of the force is centripetal, towards the cluster's centre, and from lower entropy to higher entropy.

The average irrotational horizontal acceleration for the 3 convective intensity ranges discussed in conjunction with Fig. 2, taken over pixel length of 125 m, are $5.4\ 10^{-3}$, $1.4\ 10^{-2}$, $2.2\ 10^{-2}\ m/sec^2$. As such, they are very much smaller than the first order vertical accelerations within the cloud's convective core which are O(g). The statistical distribution of the absolute value of $\vec{a_H}$ follows a basic gamma distribution whose 'scale', $\hat{a}_h$, and 'shape', $k_h$, parameters, for the full range of convective intensity, are displayed in Fig. 5.

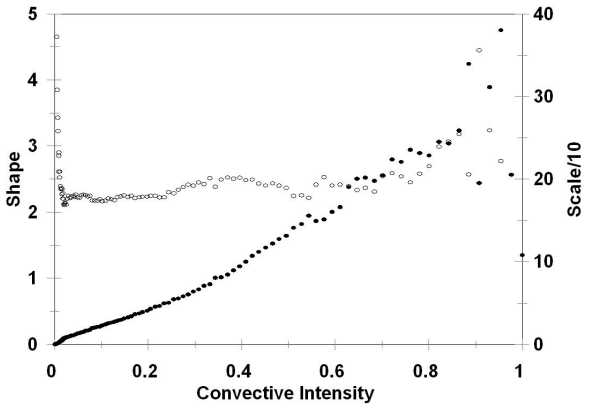


***Figure 5: Shape (open) and scale (closed) parameters for a gamma distribution fit of absolute value of the horizontal acceleration as functions of convective intensity over its entire range.***

Of special note is the wide range of convectivity where the shape parameter $k_h \approx 2$ and the scaling is a monotonic function of $\mu$. It is concluded that similarity extends to the statistical occurrence of horizontal accelerations which fit a universal gamma distribution of the form $a_h \exp(-a_h/\hat{a}_h)$ over much of the range of convective intensity.

Consider next the secondary irrotational horizontal pressure drop caused by the Bernoulli effect associated with the first order convective velocity in the core written in the form

$$\delta \vec{p}_H = \frac{1}{A_{yz}} \frac{\partial v_T^2}{\partial x} \quad (5.3)$$

where $A_{yz}$ is the common area of a face perpendicular to the x direction.

Next, consider the result of applying a horizontal divergence operator, $\partial/\partial \vec{x}$, and then invoking incompressibility at the time scales involved, such that

$$\frac{\partial}{\partial \vec{x}} \delta p_H = -\frac{\partial}{\partial z} \delta p_V = \frac{-a_V}{A_{xy}} \quad (5.4)$$

where $A_{xy} = \Delta x \Delta y = (\Delta x)^2$, we obtain the estimate for the resultant local secondary vertical acceleration

$$a_V = -\Delta x \nabla_H v_T^2 \quad (5.5)$$

This estimate in terms of the scale-weighted local horizontal divergence of the terminal velocity field is both conceptually simple and easily computed from the imagery. It also provides insight into the spatial arrangement of the modulation of first order convection in the core of clouds/ clusters as discussed below.

It is useful to examine the overall statistical distribution of the secondary vertical acceleration at the pixel level, both for its range, positive (convective) and negative (subsidence) structure, and for any difference between the statistical distributions. Fig. 6 shows the distributions at 3 convective intensities ranging from 0.1 to 0.7. The case for $\mu = 0.1$ represents almost all the pixels; $\mu > 0.5$ represents the distribution of vertical acceleration with modest convection, and $\mu > 0.7$ represents significant convection. The distributions have a larger average vertical acceleration, broaden with increasing $\mu$ skew towards convective acceleration. While such a change with increasing convectivity is to be expected, it is interesting that the range of negative acceleration increases at the same time, which is consistent with return flow and self-organized convection.

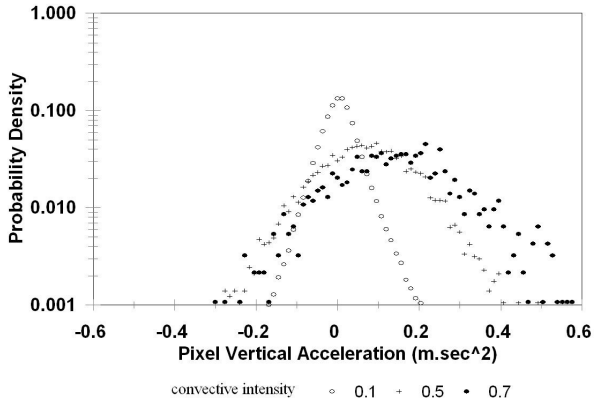


***Figure 6: Distribution of convective and subsidence acceleration within pixels for a range of convective intensity.***

## 5.1 Internal and Peripheral Accelerations of Hurricane Clusters

The net shear stress, $\sigma_{cl}$ , acting on the periphery of a cluster is found by summing the local (horizontal) rotational force around each pixel in a cluster using the weighted gradient perpendicular to that pixel face. The process of summation cancels opposing rotation of adjacent pixels, and only retains the sum of unbalanced estimates on the periphery. The result is the magnitude of the shear stress and the implied direction of rotation on the cluster's circumference. The sensitivity of the shear stress to convective intensity is shown in Fig. 7. Also note that counterclockwise rotation exists only for $\mu > 0.15$ , i.e. insignificant sensible heating. Although the associated rotational speed increases with the convective intensity, so does the variability.

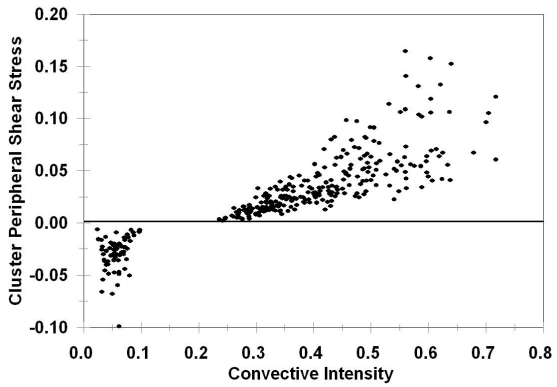


***Figure 7: Sensitivity of strength and direction of rotational shear stress on the periphery of annealed clusters with convective intensity.***

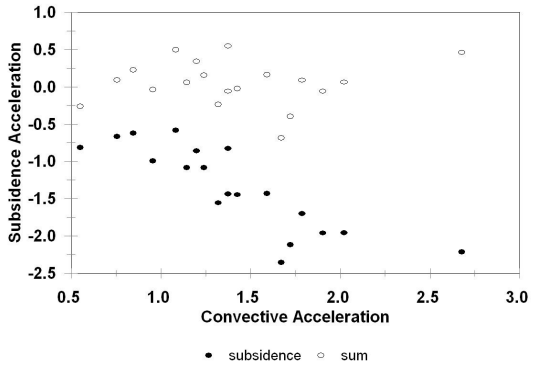


***Figure 8: Convective and subsidence acceleration summed over clusters greater than 35 pixels and their net total. The latter combined accelerations indicate individual clusters have an approximate hydrostatic balance.***

By isolating some large test clusters $(N_{pixel} > 35, \mu > 0.6)$ and examining the locations of vertical acceleration within the cluster by eye, it is apparent that all such clusters have within them convective and subsidence sub-clusters, and that there is a correlation between convective (positive upward) acceleration and positive (counterclockwise) rotation. It appears that the core of very energetic clusters is convective with subsidence localized in the outer sub-clusters. This picture of the internal cluster organization is compatible with the results of Craig and Mack ( 2013) of self-organized structure at second order.

Another test of how well-organized a cluster is at second order is whether the sum of the opposing secondary accelerations over a cluster area is more nearly 0 than each of the component accelerations. Fig. 8 presents a comparison for about 19 larger (>35 pixels) with significant convection $(\mu > 0.6)$ . There is a well defined tendency for a correlation between total subsidence acceleration and total convective acceleration in a large cluster. In addition, their sum is noticeably smaller than each component, and uncorrelated. A convenient measure of a cluster's imbalance, $h$ , in terms of the positive and negative vertical accelerations is

$$h = \frac{a_p + a_n}{a_p - a_n} \tag{5.6}$$

It is apparent that the self-organization process involving irrotational secondary vertical accelerations within precipitating columns is arranged in areas of secondary convection and subsidence to achieve optimally minimal net vertical acceleration i.e. to reduce any hydrostatic imbalance.

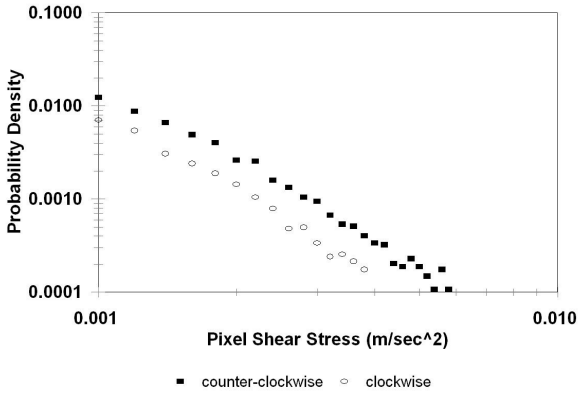


***Figure 9: Probability distribution of positive rotational shear stress of individual pixels. About 60% have no measurable rotation, and the residual is biased by a factor of 1.6 to counterclockwise rotation.***

The shear stresses of the pixels has two distinct properties – about 60% of them have negligible rotation, and of those indicating rotation there is a distinct preference for counter-clockwise direction (Fig. 9). The average ratio between the probability of counter-clockwise and clockwise directions for the clusters is about 1.6.

The net shear stress, found by integrating local pixel rotational stresses over a cluster, is equivalent to rotational acceleration $\sigma_{cl} = r_{cl}\omega_{cl}^2$ providing the estimate of the angular rotation rate,

$$\omega_{cl} = 2\pi\left(|(\sigma_{cl})|/r_{cl}\right)^{1/2} sgn(\sigma_{cl}) \tag{5.7}$$

in terms of the equivalent radius $r_{cl}=(\pi A_{cl})^{1/2}$ where $A_{cl}$ is the cluster area. The pdf of cluster shear stress is markedly different (Fig. 10) than pixel shear stress in that it is 98% positive and about an order of magnitude larger. The existence of negative rotation within the pixel field, and of only positive rotation clusters, is related to the existence of organized sub-clusters as discussed next.

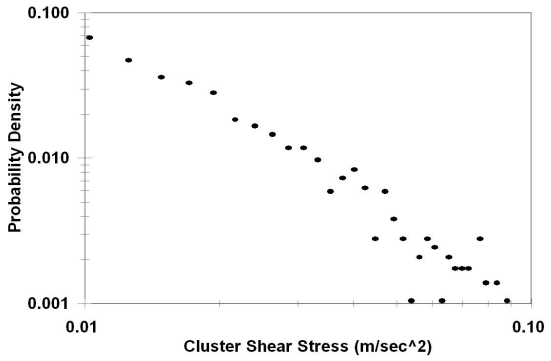


***Figure 10: Distribution of over-all cluster counter-clockwise rotational shear stress of size Npix>30 and convective intensity μ >0.6.***

## 6. Relationship of Energetics and Rotation in Convective Clusters

A simple model of the dynamical aspects of a cluster (rotation and vertical acceleration) is suggested by dimensional analysis of latent heating. If we postulate that the length and time scale for a cluster is the effective radius and its rotation rate, then by dimensional analysis

$$[\dot{L}]\rightarrow\frac{[E]}{t}\rightarrow\frac{v^2}{t}\rightarrow\frac{l^2}{t^3}\sim r_{cl}^2\omega^3 \qquad (6.1)$$

suggests the basic linkage between a cluster's latent heat production by condensation and its rate of conversion to rotational energy. Also, by the same argument, the vertical acceleration, $a_v$, by dimensional analysis, is related to $\dot{L}$ by

$$[\dot{L}]\rightarrow\frac{l^2}{t^3}\sim a_v v_{rad}\sim a_v r_{cl}\omega \qquad (6.2)$$

and by equating the two expressions, the vertical acceleration is also related to the rotation by

$$a_v\sim r_{cl}\omega^2=\frac{(r_{cl}\omega)^2}{r_{cl}}=\frac{v_{rad}^2}{r_{cl}} \qquad (6.3)$$

which also estimates a cluster's vertical acceleration in terms of its centripetal force.

### 6.1 Angular Momentum

The conceptual model which arises from the existence of counter-rotating subsidence sub-clusters in a cluster is that there is a contest for angular momentum between the counter-clockwise rotating cluster and the clockwise sub-clusters. Accordingly the observed angular momentum of a cluster is the sum of the positive and negative momentum, that is

$$\omega_{cl}r_{cl}=\omega_p r_p+\omega_n r_n \qquad (6.4)$$

and is less than $\omega_p r_p$ generated by the latent heating alone. It is reasonable to assume that the source of negative rotation is the dissipation rate as it removes ultimately rotational energy. If we consider the latent heating and dissipation within both the positive and negative rotating areas, an estimate of the ratio of positive and total angular momentum, defined as $r_{mom}$ is

$$r_{mom}=\frac{(\dot{L}_p r_p+\dot{L}_n r_p)^{1/3}}{(D_p r_n+D_n r_n)^{1/3}}=\left(\frac{r_p}{r_n}\right)^{1/3}\left(\frac{\dot{L}_p+\dot{L}_n}{D_p+D_n}\right)^{1/3}=Y$$

$$Y=\left(\frac{r_p}{r_n}\right)^{1/3}\left(\frac{\dot{L}}{D}\right)^{1/3}=\left(\frac{r_p}{r_n}\right)^{1/3}\mu^{1/3} \qquad (6.5)$$

where p and n denote the positively and negatively rotating areas, of effective radius, $(r_p,r_n)$, of energy generation, $(\dot{L}_p,\dot{L}_n)$, of energy removal, $(D_p,D_n)$, and of total energy rates within the cluster of $(\dot{L},D)$. The total positive angular momentum of the cluster is $\omega_p r_p$ and the total angular momentum available for removal is $\omega_p r_p-\omega_n r_n$, leading to the relationship

$$\frac{\omega_p r_p}{\omega_p r_p-\omega_n r_n}\sim\frac{\omega_p r_p}{2\omega_p r_p-\omega_{cl}r_{cl}}\sim\left(\frac{r_p}{r_n}\right)^{1/3}\mu^{1/3} \qquad (6.6)$$

The hypothesis that the ratios of momentum are related to the convectivity was tested for 14 clusters, of size $N_{pix}>25$, and hydrostatic imbalance, $h<0.12$. The ratio of estimates from direct calculation involving angular rotation rates of the positive and negative sub-clusters, and the cluster's convective index are shown to be approximately equal in Fig. 11. The best fit ratio is 0.66 +/- 0.026, which is both of the order of 1, and has small variability over the range of $\mu$

.

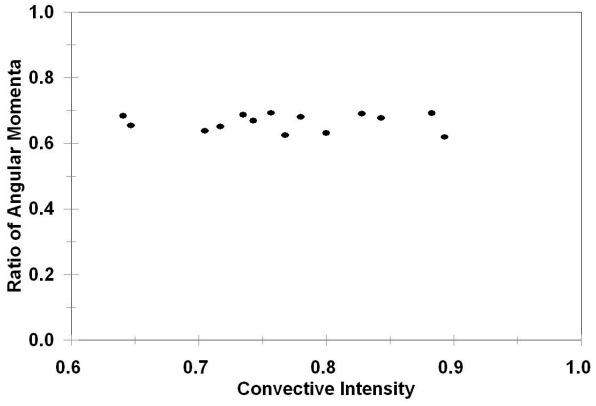


***Figure 11: Ratio of positive rotational momentum to the total (absolute) rotational momentum in a cluster compared to the ratio of positive and negative momentum associated with the convective intensity.***

An empirical fit of the positive angular momentum as a function of $\mu$ ,

$$\frac{\omega_{cl} r_{cl}}{\omega_p r_p} \approx 0.5 + 0.67(\mu - 0.6) \quad (6.7)$$

was found, as well as an empirical estimate for the relative size of the positively and negatively rotating sub-clusters, given by

$$\frac{r_n}{r_p} \approx 0.5 + 1.25(\mu - 0.6) \quad (6.8)$$

for clusters with negligible hydrostatic imbalance, $|h| < 0.055$. Together they provide a model for the size and rotation rates of the positive and negative sub-clusters as a function of $\mu$. Interestingly, Eq. 6.8 predicts that the negatively rotating sub clusters increase to match those positively rotating in the limit where the production matches the dissipation of energy, that is $r_n \to r_p \to 0.5$ as $\mu \to 1$. The explicit effect of a larger hydrostatic imbalance on these relationships could not be found, except to note that it appears to be significant.

## 7. Height Dependence of Energetics and Rotation

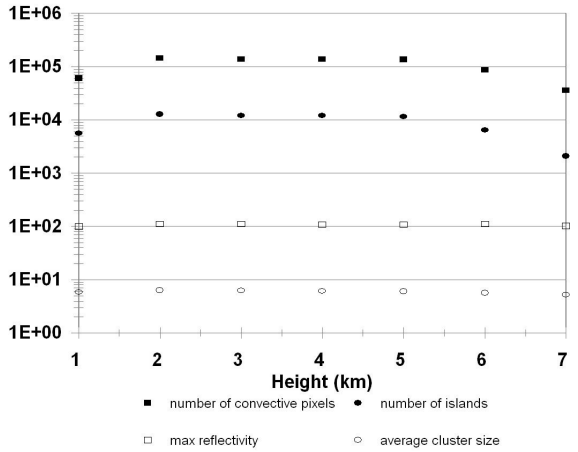


***Figure 12a: Height dependence of number of convective pixels, clusters, maximum reflectivity and average size of clusters.***

The previous analysis of the properties of clusters in a hurricane was limited to a single height. Much is known of the structure, both horizontally and vertically, within such clouds. What is not understood is the interplay between individual clouds in determining the spatial average of the field of convection. The results of the descriptions in previous sections, of some of the energetics and rotation properties of clusters lead to the basic question: what is the net effect, both horizontally and vertically, of the localized semi-coherent convective process, occurring randomly in its initiation time, and location?

The procedure which was followed first annealed the Irma hurricane image, described above, at 7 levels from 1000 to 7000m. Various statistics of the overall field at both the pixel and cluster scale were assembled and are described. A location within an image is described as convective if its convective intensity, $\mu_{cr} > 0.17$, the threshold for latent heating to exceed sensible heating, as described in Section 2.2. Some basic results are provided in Figs. 12a for the vertical structure of horizontal averages at a given height of the number of sufficiently convective pixels, of the number of annealed clusters, of the maximum reflectivity and the average size of all clusters.

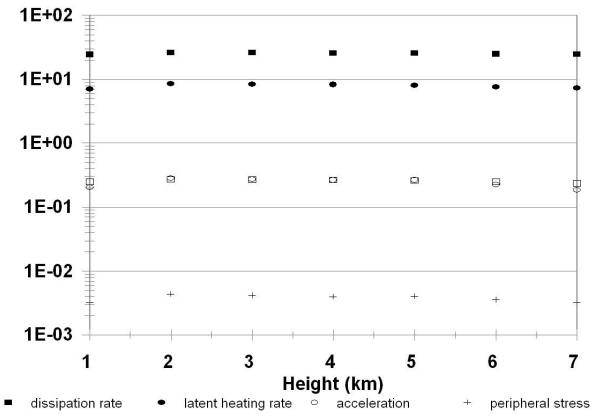


***Figure 12b: Height dependence of dissipation and latent heating rates, vertical acceleration and peripheral stress.***

The most striking result in Fig. 12a is presence of the nearly constant structure for the relevant process parameters - maximum reflectivity and cluster average size, particularly from 2 to 5000 m. Their near constancy implies that the convective process, despite its localization in clusters, is acting coherently vertically, and that image properties observed at 2000m are almost identical to the same property up to near maximum cloud-top levels. This result also offers confirmation of the annealing process to identify clusters in that it returns almost the same number of clusters and the same average cluster size through this core of the hurricane's convection.

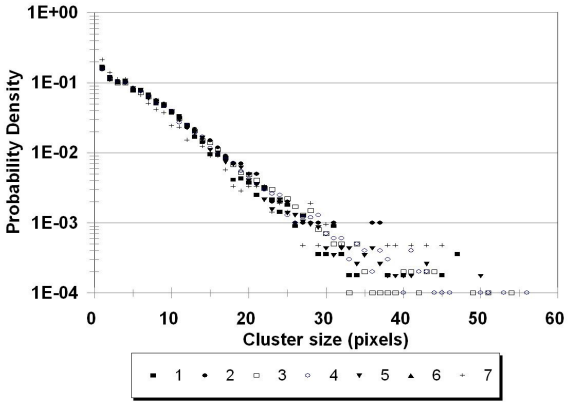


***Figure 13: Probability density function of clusters at various heights (km).***

Fig 12b provides more detailed properties of the cluster structure, specifically the average convectivity, latent heating, dissipation, vertical acceleration and peripheral stress. Again they are all essentially invariant through the convective core, with small decreases on the lowest and highest levels. It could be argued that the constancy is related to constancy of the reflectivity because basic similarity can be traced to it. However that could not explain the spatial arrangements of energy and convective intensity which define the entropic

force field. For the average vertical acceleration and shear stress/rotation rate to be the same vertically requires that the derivative field around pixels is solely a function of the reflectivity at that pixel which is exceedingly implausible. It is concluded au contraire that the constancy of both the reflectivity and the energetics and rotation are constant through the convective core as part of a basic property of the cluster field.

Clearly the structure within clusters at different heights is related to the constant convectivity layer. Accordingly the probability density distribution of the clusters on each level were computed and displayed as a function of height in Fig. 13. The distributions inherently posses the same invariant structure – they are very similar in the constant convectivity layer and deviate slightly at the bottom and top levels. The negative exponential structure was discussed in Sect. 4. The best fit to all heights, in the form

$$pdf(A) = \alpha \exp(-\beta A) \quad (7.1)$$

is $\alpha \approx 0.74$ and $\beta \approx 9.5$ where the area is expressed in km$^2$.

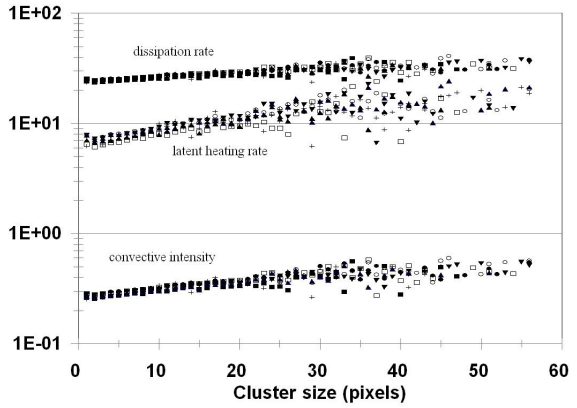


***Figure 14: Average dissipation and latent heating rates (W) and convective intensity as a function of cluster size and height.***

Now consider the energetics associated with clusters at different heights. Fig. 14 presents the average latent heating, dissipation and their average ratio over the clusters at that height. A logarithmic axis has been chosen to be able to contrast them on one graph, as well as examine their ratio. All three increase with larger clusters as might be expected. The variation of dissipation, based solely on estimates of terminal velocity, increase with a constant slope. However the slope of the convectivity changes noticeably for clusters greater than about 30 pixels (0.5 km$^2$). The same break point occurs in the distribution of latent heating indicating that the change is associated with errors in the estimation of $\mu$ and/or its use in the annealing process.

Fig. 14 also demonstrates that the convectivity is increasing as a result of increasing latent heating, and not decreasing dissipation, and that the break in $\mu(A)$ stems from the reduced average latent heating in large clusters. As mentioned above, this effect may not be real, but some feedback error associated with the clusters, annealed under local pixel $\mu$, which are slightly too large.

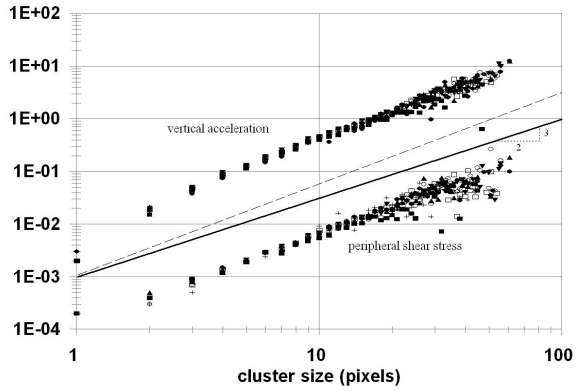


***Figure 15: Average vertical acceleration and peripheral shear stress (m/s^2) as a function of cluster size and height.***

Fig. 15 compares the vertical acceleration and shear stress with cluster sizes. In this case there is a different sensitivity, with cluster area based on linearity of the log-log plot, to a power law relationship, i.e.

$$(a_v, \sigma) \sim A_{cl}^{\gamma} \quad (7.2)$$

where $\gamma \approx 1.7$ based on the entire range of cluster areas. Accordingly the key dynamic factors, vertical acceleration and shear stress increase faster than the rate of increase of cluster area. Apparently large convective clusters have an internal structure such that they can accelerate their vertical acceleration and rotation speed. An argument for a $A^{3/2}$ structure of Eq. 7.2 is readily derived from a dimensional analysis given by

$$(a_v, \sigma) \rightarrow l t^{-2} \sim A^{1/2} \omega^2 \quad (7.3)$$

if $\omega \sim \eta A^{1/2}$ where $\eta$ is scale independent.

To be definitive about the actual sensitivity to cluster size requires evaluating the annealing algorithm for systematic overestimation of $A$ as mentioned above. Whatever the exact rotation rate sensitivity to scale, the fact that it exceeds linear, argues for an unstable cycle of yet more vertical growth, more entrainment, a larger cross-sectional area, and a further increase in rotation rate with cluster area growth.

## 8. Internal Hurricane State

Hurricane category, usually estimated on the basis of wind speed and core pressure, reflects the synoptic energetics of a hurricane. (Similarly, tornado category is based on sustained wind speed of the vortex.) Next a method is sought which indicates the current state of an evolving hurricane (or tornado) on the basis of the 'micro-scale' energetics of its clusters.

Classically, two parameters are required to characterize rotating convection. The first is the Rayleigh number, which parameterizes the convective heat flux in terms of an external mean vertical temperature gradient, and the second is the Ekman number, which characterizes large scale vorticity. By extension, two non-dimensional balances involving rotating cluster energetics are required to represent a hurricane (or tornado's) internal cluster state.

In addition to measurements of wind speed and pressure, the notion of the texture of the cloud field is also cited in recognizing a hurricane's category. Here that concept of texture is shown to be suitably represented by the size distribution of the clusters constituting a hurricane/tornado.

The convective state of a cluster is represented by its convective intensity, $\mu$ , which characterizes the relative rates of energy exchange involving latent heating, $\dot{L}$ , and dissipation, $D$ , (in the terminal velocity field), i.e

$$\mu = \dot{L}/D \qquad (8.1)$$

It is suggested that a natural parameter to characterize rotation of a cluster is the ratio of momentum involved in the angular momentum of a rotating cluster and the terminal velocity of the field of the precipitation within the cluster, and i.e.

$$\psi = \frac{r_{eff}\,\omega}{v_T} \qquad (8.2)$$

(Another choice, the ratio of a cluster's rotational acceleration, $r_{eff}\,\omega^2$ , to its vertical acceleration, $a_v$ , could also be considered.) In addition, a simple variable which characterizes texture of an image is the scale size of a (negative exponential) distribution of cluster sizes, $A$ . That distribution can be shown to be a function of the state/age of a cluster field.

These parameters are not independent. For example, as dissipation is defined by $D = g\,v_T$ , $\mu$ and are both explicit functions of $D$ . In addition, both $\mu$ and $\psi$ are functions of $A$ .

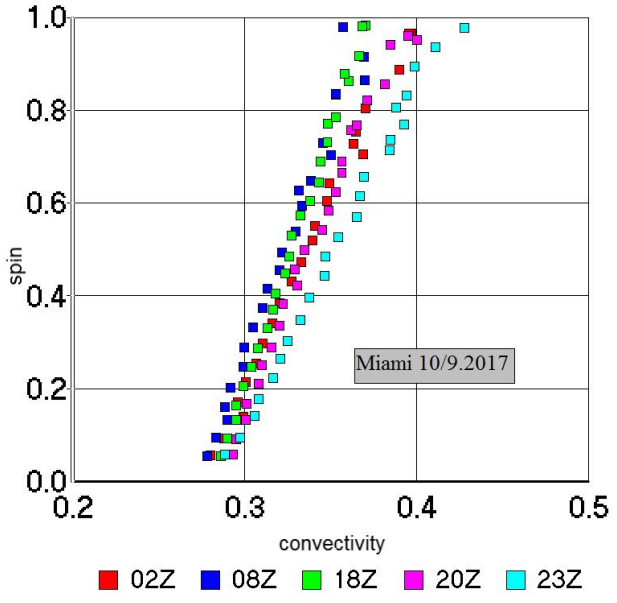


***Figure 16: 'Spin' versus 'connectivity' during 2017/09/10 as seen by the Miami radar.***

## 8.1. Definition of Internal Hurricane State

As shown in Figure 16, the ratio of the rotational speed to the average vertical terminal velocity of t precipitation within an annealed cluster, called the 'spin', is proportional to the cluster's ratio of latent heating to dissipation, called 'convectivity'. Above spin, $\psi = r_{eff}\,\omega / v_T = 1$ , the slope is maintained but the scatter increases. The maximum displayed value of connectivity represents the condition when the horizontal rotation speed equals the average speed of rain falling through the cluster at that height (3km).

It is useful to capture the shifting of each hour's averaged slope by estimating the value of the convectivity, $\mu = \dot{L}/D$ , at $\psi = 1$ , denoted $\mu_1$ .

Between 02Z and 08Z, as Irma moved away from the coast of Cuba, its intensity increased. On Fig. 16, that corresponds of the characteristic shift to the left, i.e. to less convectivity. Physically, that shift is interpreted that, as the hurricane strength increases, less convectivity supports more rotation. Since the decrease in $\mu_1$ is counter-intuitive to characterizing increasing hurricane intensity, $\zeta$ , it is useful to define its inverse as the internal hurricane state, i.e

$$\zeta = \frac{1}{\mu_1} \qquad (8.3)$$

## 8.2 Time variation of Internal Hurricane State

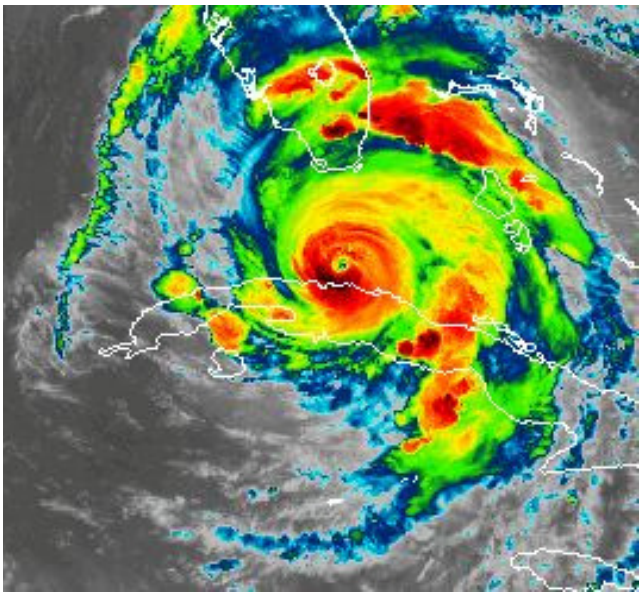

***Figure 17a: Irma 2017/09/10:10Z Category 4 (2.65)***

Fig. 17 helps visualize the time variation of Irma, as seen by the Goes 16 satellite, at four distinct stages of its evolution. The first, 17a, occurred when Irma had moved out from the coast of Cuba and had been measured by aircraft as a Category 4 hurricane on the Saffir-Simpson scale. Note its tight, closed structures with well-defined sub-features. The second image, 17b, occurred as Irma was about to move onshore between Fort Myers and Marco Island. It is somewhat larger and more diffuse than 17a. but retains its dark core. After moving very slowly on-shore and beginning

its journey up the Florida peninsula (Fig. 17c), Irma was considerably more dispersed but still retained a smaller dark intense core. By the time that Irma had reached Georgia (Fig. 17d), it had lost is core and the previous strong rotation and the banding structure had weakened considerably.

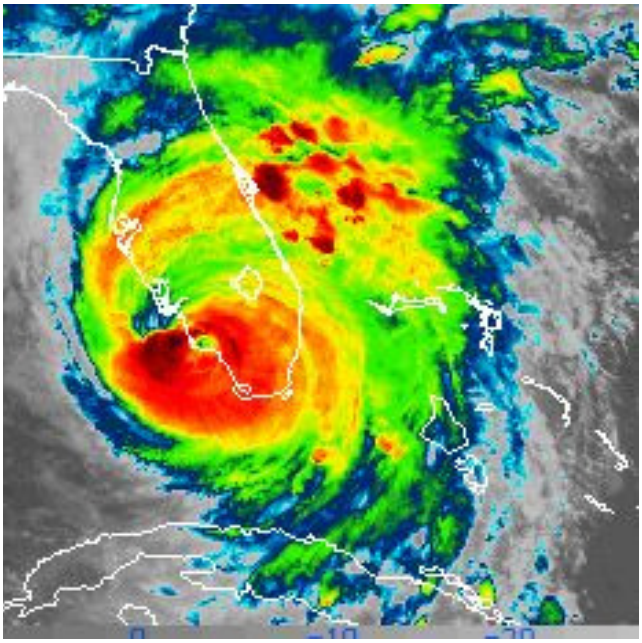

*Figure 17b: Irma 2017/09/10:20Z Landfall - Category 3 (2.7)*

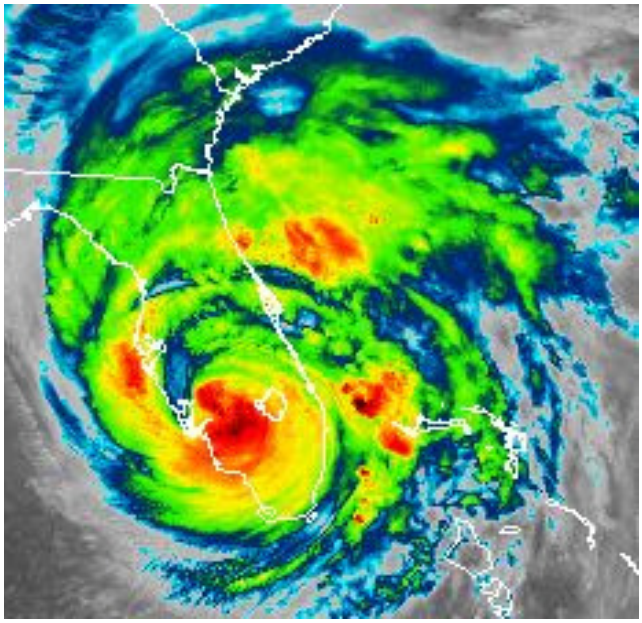

*Figure 17c: Irma 2017/09/11:00Z Inland , moving north (2.4)*

The estimated hurricane state (discussed next), based not on the aircraft measurements, but on ground-based radars imagery, has been placed in the figure captions of each image.

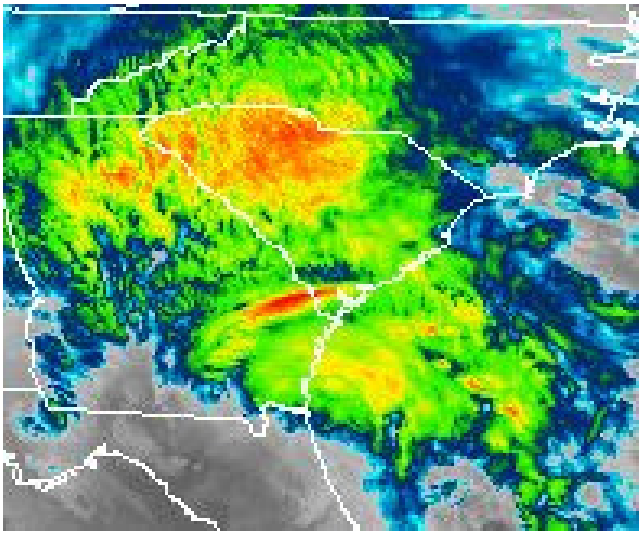

*Figure 17d: Irma 2017/09/11:12Z Dissipating-Tropical Storm over Georgia (1.9)*

## 8.3 Observed Hurricane State

The variation with time of $\zeta$ for the passage of Irma from 2017/09/10:00Z to 2017.09/11:23Z, captured in Fig. 17, is presented in Fig. 18. The output represents hourly averages of radar scans (at 3 km height) at about 7 minute intervals.

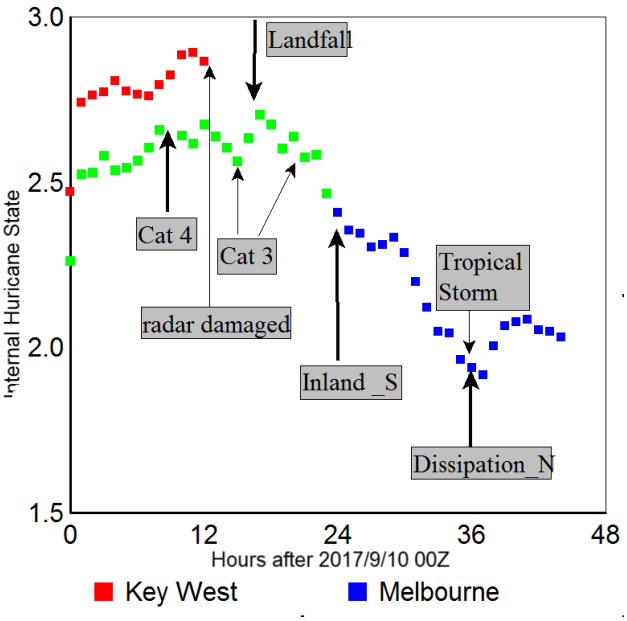


*Figure 18: Time variation of internal hurricane state at 3 radar sites (Key West, Miami and Melbourne Fl.)*

Several labels have been place on Fig. 18 to indicate Irma's evolving status – its hurricane category as determined by the National Hurricane Center, and the occurrence of key events. Several features stand out. The first is that the Key West radar operating at the same time as the Miami radar indicates a higher internal hurricane state at all common times. A plausible reason for the discrepancy is that Miami was not detecting the hurricane beyond its active core but Key West was. Note that the 2 radars – Miami and Melbourne – show no sign of a displacement in hurricane

state at their common time. The difference in this case and the first involving Key West may be that Irma was essentially between the Miami and Melbourne radars, and presumably was sensed similarly by both radars.

It is observed that, according to the Miami radar, the S-S hurricane category was actually above Category 4 when it came ashore – which was not observed by analysts as there was not an aircraft sounding at the time.

In Fig. 18 the internal hurricane scale varies consistently with the known/physically observed S-S hurricane categories in that it produces the same estimates for $\zeta$ when the two Category 3 occurrences were observed.

Lastly, the change in the internal hurricane state is dramatic (and linear) in the dissipation stage, ('S' to 'N' designations) but more subtle (but observable), with gradual changes in S-S categories until it reached tropical storm status.

From Fig. 18 it is possible to tentatively conclude that the internal hurricane state, $\zeta$ ,
a. follows the S-S hurricane categories faithfully, on an hourly basis and
b. suffers from underestimation if the radar is not sampling the entire convective area.

As a result it is recommended that a similar method be developed using satellite data, particularly from Goes etc imagers, which capture the entire hurricane and can follow the evolving hurricane in far off-shore locations. However it remains to be proven that the computation of the internal hurricane state using satellite imagery, instead of radar imagery, is possible.

## 9. Conclusions

### 9.1 Major Results

1. There exists a similarity structure of the large-scale energetics of a hurricane.

2. Existing methods of deriving physical variables, particularly terminal velocity of rain, drop radius, and the rain rate, lend themselves to an evaluation of energetics at the pixel scale.

3. A key variable, applicable at various scales, is the convective intensity, which acts as a similarity parameter, for a similarity theory of moist convection.

4. The convective intensity is derivable from measurements of the rain rate or from an informational entropy process involving nearest neighbour differences in energy.

5. Simulated annealing of the hurricane radar image using the convective intensity produces a field of spatially independent clusters.

6. The application of entropic forces, first at the pixel resolution, and then integrated over a cluster, produce estimates of vertical accelerations and rotation of a cluster.

7. The energetics of a cluster is explicitly tied to its angular momentum.

### 9.2 Future Research

1. Evidence exists of a modified form of Richardson dispersion within the hurricane's cloud field.

2. To be able to trace individual clusters with time and height, a probit analysis involving invariants
associated with the energetics and angular momentum, is being pursued.

3. The influence of the overlying thermal stratification on the rotation of clusters needs to be clarified.

4. An ideal application of this research is to monitoring the 'hurricane state' based on its energetics, either by a ground or possibly a satellite radar.

## Appendix A: Connectivity, Nearest Neighbours and Informational Entropy

The field of hurricane, driven by latent heating and dissipated, in the turbulent droplet motion within a cloud is a mixture of spatial order and disorder; one that varies with the convective state. To understand cloud morphology in the context of the imagery, new methods are required to describe the fields in terms of the information contained in its texture and structure. By examining either the connectivity of nearest neighbours, or the extended connectivity beyond nearest neighbours, it is possible to identify local conditional variability and sinuosity respectively. Whatever the approach, the method invariably utilizes recursive searches for paths of increasing or decreasing energetics, e.g. energy or entropy change, or for objects like boundaries/walls/paths in the convective milieu. Here only a specific nearest neighbour analysis is outlined because a very specific result is sought.

### A.1 Computation of Convective Intensity

One property which has proven useful (e.g., Kerman, 1998; Kerman et al., 1999) in a characterization of the chaotic images of a geophysical field is in terms of the conditional probability of the difference of some measure of energy between a pixel and its neighbour. Specifically, consider the conditional probability of neighbouring pixels with an energy difference between them expressed as $\delta v_T^2$ (see Eq. 3.10). Operationally, neighbours are considered across 8 vertex/face positions around a (square) base pixel, conditional on the energy difference, for negative differences, i.e. the neighbouring energy is smaller. The resulting conditional probabilities are based on the convective intensity, or equivalently, the reflectivity of the central pixel.

The informational entropy, $\chi_{cond}$ , given by

$$\chi_{cond} = -\ln p_{cond} \qquad \text{(A.1)}$$

was computed from the conditional probabilities. The slope of the conditional probabilities with energy for a given relectivity $R$ are fitted by

$$\frac{\partial v_T^2}{\partial(\beta \chi_{cond})} = \mu \qquad \text{(A.2)}$$

as a function, $R$ . $\beta$ is a constant which is associated with the fact that $\chi_{cond}$ is an informational entropy, and not the physical entropy, S, involved in Eq. 3.10. A simple

proportionality assumption between them is reasonable as it is the energetics creating physical entropy, S, which also creates a chaotic spatial structure associated with the informational entropy, $\chi$ . To determine $\beta$ and isolate $\mu$ , the observed slope $\partial v_T^2 / \partial \chi_{cond}$ is normalized by its maximum value (~15) at $R_{max}$ so that the resulting scaled slope is associated with $\mu_{max} = 1$ .

The empirical results for $\mu$ determined in this way are compared to values determined by application of the rain rate model (Eq. 3.3). The results are surprising good: in fact almost identical for the range of reflectivity, $R$ , in the deep convective state. Otherwise they are less than what the rain rate model predicts. The immediate question is which structure, if either, is correct. Because the validity of a simple proportionality, $\beta$ , between the different entropies, is supported by the agreement between the predictions in the deep convection state, and a change in the energetics, as argued in Sect. 1, is believed to exist there, a change in $\mu(R)$ between convective states is probably more realistic than the monoslope rain rate model.

The form of the conditional probabilities of neighbouring energy is typical of systems in which the energy is spatially and stochastically distributed. The model developed here is a statistical dynamics analogy in terms of energy distributed throughout the image of the hurricane. From Eq. 3.10, the model equates entropy with $\mu^{-1} v_T^2$ whereas the classical thermodynamics model of atomic physics has a similar form, $(k_b T)^{-1} v_{mol}^2$ , in terms of the kinetic energy of atoms and molecules and temperature, $T$ . By analogy, the convective intensity is the equivalent of $k_B T$ in a mixture of convective structures within the hurricane. Contrary to a classic statistical physics process which is homogeneous with a common temperature, the transfer of energy towards dissipation and dispersal in a hurricane is distinctly non-homogeneous with the internal (cloud) structure itself highly variable over the range [0,1] of the convective index

## References


Battan, L. J., 1973: Radar observation of the atmosphere. The University of Chicago Press, Chicago, 324 pp.

Bister, M., and K. A. Emanuel, 1998: Dissipative heating and hurricane intensity. *Meteor. Atmos. Phys.,* 65, 233–240.

Craig, G. C., 1996: Dimensional analysis of a convecting atmosphere in equilibrium with external forcing. *Quart. J. Roy. Meteor. Soc*., 122, 1963–1967.

Craig, G.C. and J. M. Mack, 2013: A coarsening model for self-organization of tropical convection. *J. Geophys. Res., Atmospheres*, 118, 8761–8769.

Emanuel, K.A. and M. Bister, 1996: Moist convective velocity and buoyancy scales. *J. Atmos. Sci.,* 53, 3276–3285.

Kerman, B.R., 1998: On the relationship of ice pack thickness to the length of connectivity trees in SAR imagery. Proc. 14th Int. Symp. on Ice in Surface Waters, vol 2 (H.T. Shen, ed.), 811-819. Clarkson Univ., Potsdam, N.Y.

Kerman, B.R., P. Wadhams, N.R. Davis, J. Comiso, 1999: Informational equivalence between synthetic aperture radar imagery and the thickness of Arctic pack ice. *J. Geophys. Res.*,104(C12), 29721-9731.

Kleidon, A., 2010: Non-equilibrium thermodynamics, maximum entropy production and Earth-system evolution. *Phil. Trans. R. Soc. A*, 368, 181–196.

Mali, P., S. K. Sarkar and J. Das, 2003: Raindrop size distribution measurements at a tropical station. *Indian Journal of Radio & Space Physics*. 32. 296-300.

Pauluis, O., and I. Held, 2002; Entropy Budget of an Atmosphere in Radiative–Convective Equilibrium. Part II: Latent Heat Transport and Moist Processes. *J. Atmos.. Sci.*, 59, pp 140-149.

Press, W.H., B.P. Flannery, S.A. Teukolsky, and W.T. Vetterling, 1989: Numerical Recipes in Fortran. Cambridge University Press. 722p.

Richardson, L. F., 1926: Atmospheric diffusion shown on a distance-neighbour graph. *Proc.Roy. Soc. Lond. A* 100, 709-737.

Rogers, R. R., 1979: A short course in cloud physics, Pergamon Press, New York, 2nd edition, 235.

Simpson, J., 1972: Use of the gamma distribution in single-cloud rainfall analysis. *Mon. Weather Review*, 4, 100-103.

Tao, W.-K., C. H. Sui, B. Zhou, K. M. Lau, and M. Moncrieff, 1999: Equilibrium states simulated by cloud-resolving models. *J. Atmos. Sci.,* 56, 3129–3139.


## Acknowledgements


The author would like to thank Professors Emeritus Roger Pielke, Colorado State University, and Douw Steyn, University of British Columbia, for their support and encouragement.